SCIPEDIA

Eddy Current Modeling and Simulations for the Characterization of Low Thickness Multilayer Materials

Salim Bennoud* and Elkhahina Sari

Institute of Aeronautics and Space Studies, University of Blida 1, Blida, 09000, Algeria

INFORMATION

Keywords:
Eddy current
finite element method modeling
multilayer structures
impedance measurements

DOI: 10.23967/j.rimni.2024.10.56089

SCIPEDIA Revista Internacional de Métodos Numéricos para Cálculo y Diseño en Ingeniería

RIMNI Revista Internacional Métodos numéricos para cálculo y diseño en ingeniería

Eddy Current Modeling and Simulations for the Characterization of Low Thickness Multilayer Materials

Salim Bennoud* **and Elkhahina Sari**

Institute of Aeronautics and Space Studies, University of Blida 1, Blida, 09000, Algeria

ABSTRACT

Measuring and determining the parameters and characteristics of multilayer structures have become an important subject for several recent studies. This importance is due to industry needs and structural health requirements. The eddy current inspection is considered an important practical tool that ensures the safety and efficiency of multilayer structures and responds to the above necessities. The diversity of multilayer structure characteristics is one of the principal problems that must be solved. These physical and electromagnetic parameters are not always available or provided by the suppliers. Another problem that arises in the development of different models related to these structures is the difficulty of obtaining a satisfactory diagnosis. This difficulty returns to the complexity of geometry, the presence of small dimensions and sizes, and the existence of various parameters. In this context, it is necessary to achieve a strategy for the development of software and hardware tools concerning the characterization of multilayer structures. These tools must be applied to surmount the above problems and improve the technical advantages of the eddy current inspection. The principal objective of this work is to investigate the efficacy of the eddy current method applied to aeronautical materials, particularly low thickness multilayer structures. The modeling was performed using the finite element method. A software program was developed to investigate changes in the coil impedance. Results are initially validated and compared against the analytical and computational results given for simple cases. They are very similar, and they present a good agreement for both situations. The error is 5% for the calculus of the induction magnetic B. It also varies from 0.17% to 5.32% for impedance responses that enable the application of the developed code to carry out simulations for complex geometries. For various values of parameters and a wide range of applications, the parameters and properties of the problem can easily be introduced into the code. This permits the analysis and calculation of changes in impedance versus the effect of any variation in parameters. The developed approach is sufficiently general. It can simulate various potential cases of defects in low thickness multilayer structures due to its adequate design. It can generate interpretable results for different

OPEN ACCESS

Received: 14/07/2024

Accepted: 02/10/2024

DOI
10.23967/j.rimni.2024.10.56089

Keywords:
Eddy current
finite element method modeling
multilayer structures
impedance measurements

*Correspondence: Salim Bennoud (bensalimen2006@yahoo.fr).

defect lengths and locations based on its fast computation and its ability to plot impedance responses. In addition, it can be used as a useful tool to assist students, engineers, and researchers in improving programs and materials related to eddy current inspection.

1 Introduction

Thin multilayer structures are extensively used in different engineering applications, e.g., aeronautical assemblies, materials covered by an insulator, overlapping metallic sheets, coated metallic plates, laminated materials, etc. [1–4]. The determination of all properties of multilayer structures depends considerably on the thickness of the constructive layers of the desired structure. These properties (principally, the electromagnetic, mechanical and physical properties) directly affect the electromagnetic signals [1].

The main elements of the aircraft structure consist of thin aluminum sheets. The application of rivets, fasteners, or welding ensures the attaching and overlapping of these sheets to the fuselage or multilayer joints. A thin gap generally separates these multilayer structures. This gap may be a favorite place where various defects, such as fatigue cracks and corrosion, can occur. These defects are serious problems of the in-service aircraft structure, which affect its airworthiness and even result in its total loss [5,6].

The physical and mathematical modeling of a multilayer structure with or without defects is always complex and difficult. These difficulties are mainly related to various factors, such as the complexity of geometry, the presence of small dimensions and sizes, and the existence of various parameters. On the other hand, the characteristics of the material are not always available or given by the suppliers.

The principal objective of this work is to investigate numerically the efficacy of the eddy current method applied to aeronautical materials, particularly low thickness multilayer structures. However, assessing and controlling materials and structural health, especially for thin multilayer structures, are key points for ensuring the durability, safety and reliability of structures. It is therefore necessary to characterize materials and defects and identify the sensitive parameters that can increase control performance. In this aim, it is important to achieve a related development of software and hardware tools concerning these problems. These improvements can include the development of self-designed tools or the performance enhancement of existing tools.

Recently, there have been many works, which focus on defect detection and propagation as well as the material characterization of a multilayer structure. Various techniques can be used to improve detection efficiency and analysis reliability. Many studies prove the diversity of techniques and explore the results issued and obtained from these techniques, such as thermographic testing, ultrasonic techniques, X-rays, etc.

Ultrasonic nondestructive testing can be used to determine residual stresses. This method has an appreciated depth of penetration, which is more important than other nondestructive techniques. It cannot detect cracks in multilayer structures due to its requirement to use a coupling agent [7]. Pulse infrared thermography can effectively estimate the size and depth of defects. It is a non-contact testing with high inspection speed [8,9]. X-ray testing can efficiently detect hidden cracks, but it has negative effects on the human body [9]. The application of eddy currents testing can be more significant with the reduction of the excitation frequency and the increase of the eddy current skin depth. The use of a TMR (tunnel magneto-resistance) sensor for example can achieve this improvement [10].

Among all the existing methods of non-destructive testing (NDT) eddy current (EC) methods are frequently the most appropriate for the control of metallic structures or components. They are very practical methods in advanced engineering fields such as nuclear, aeronautic, automobile, aerospace and other industries. They are commonly used to assess and characterize a large class of conductive materials.

However, the EC method is always considered as a reliable and effective method. Generally, it can be used to measure the layer thickness, characterize the difficulties of the layer access, and determine the stripping areas and riveting failures. In addition, it can inspect a particular layer in a multilayer structure and subsurface defects such as cracks, corrosion, air gaps, etc. [11–14]. In the field of the aeronautic industry, the EC method is currently applied for over 50% of all aeronautical inspections and controls [5,14–18]. It is successfully applied to solve specific problems in this field compared to other techniques. These problems, such as the detection of hidden defects in multilayer structures and the detection of metal thinning due to corrosion propagation are complex. Thus, it is frequently used for measuring and clarifying the coating thickness and real condition of a major part of the aircraft structure [19–22].

In the last decades, various studies concerning the detection and localization of defects in aeronautical structures have been presented. Among the published works, many studies aim to improve detection efficiency by increasing qualitative and quantitative analysis. This improvement is achieved using various EC techniques such as Pulsed Eddy Current (PEC), Multifrequency Eddy Current (MED), Eddy Current Array (ECA), and Sweep Frequency EC. In addition, it strongly depends on the development of numerical simulation methods, which is a significant way to improve the diagnostic process [22–25].

For several years, rigorous progress has been made in the computation of electromagnetic fields, including the modeling of EC problems. This progress is appreciable for understanding and analyzing the changes in impedance responses. The impedance changes are directly related to the existence of defects or modifications in configuration properties. However, any small impedance variations due to these changes and the inspection process must be captured in any suggested model.

Several analytical, experimental and numerical approaches used to calculate the impedance variation during scanning over a multilayer structure were early developed and used. The sample can have any number of layers, and the studied configurations fall into two principal fields: the planar layers and the coaxial cylindrical layers. Analytical models of the EC problems, especially for planar multilayer cases with constant electric and magnetic properties, are well developed in several References [26–28]. The works presented in [29,30] discussed relevant analytical models for appropriate configurations with changeable properties. Recently papers investigated expansions of the Dodd model, which may present some numerical difficulties. These difficulties are surmounted using a technique that replaces the integral form with series expressions. This approach can readily reduce the time consuming of resolution and control the calculation error [31].

Nonetheless, these analytical approaches present some limitations for solving real industrial problems, mainly their incapability for solving complex problems. On the other hand, various methods (semi-analytical or numerical) are more practical to solve complex problems. This is due to their ability to model real problems associated with their complexities. Results from various papers numerically investigated the impacts of geometry complexity, nonlinearity of material and defect characteristics, and other complexities.

Various numerical methods have been applied to calculate the EC response. These methods include the finite difference method, the boundary element method (BEM), and the finite element method

(FEM) [32–35]. Among them, the finite element method FEM has been used for a variety of EC-NDT problems [36–38]. Results from these works show that parameters such as material type and condition, surface finish, probe conception, and many other factors can affect control sensitivity.

The delicate point of the EC testing is its incomplete penetration into the multilayer structure. The excised magnetic field generated by the probe offsets the magnetic field attached to these currents. This effect decreases the EC density as the depth increases. For behavioral reasons, the probes and the control parameters must be optimized to obtain maximum penetration [39].

This paper focuses on the exploitation of a computational model based on the FEM method. This computational model can calculate the interaction between a multilayer structure and an EC probe. The multilayer structure consists of several mediums in the presence or absence of a defect, and the EC probe emits a controlled excitation field.

In this work, the probe response, distinguished as the impedance changes due to its displacement above a plated sample of aluminum alloy, is carried out. The solution consists of the implementation of the FEM model through a self-designed program and the exploration of numerical data to investigate impedance changes.

First, the computational and theoretical results are compared and validated. Next, from the calculated parameters (real and imaginary components of the impedance) the influences of related characteristic parameters can be deduced and determined. These characteristic parameters can be used to understand the probe responses and the influence of the defect and configuration parameters on these responses.

Various parameters that describe the considered problem and characterize the defects and/or hidden discontinuities are investigated in the same algorithm. Many previous studies provided solutions that only interested in a limited number of parameters (one in general). The code performance is discussed through different applications according to various values of parameters and a large range of frequencies.

2 Method

2.1 Problem Description

The geometrical characteristics of the problem are similar to a traditional configuration of eddy current non-destructive testing EC-NDT. An appropriate coil is located above the target sample that consists of two layers separated by a thin layer (gap). The coil is placed on the upper layer, and defects can be located at different depths. This model corresponds to that of a coating on a wing rib or spar possibly separated by an air-gap of very thin thickness. The electromagnetic properties in each region are assumed as isotropic, homogeneous and linear. The assumed conductivity and permeability are respectively denoted by σ_i and μ_i (i = 1, N) from the upper layer to the bottom layer N.

This configuration enables the study of the effect of various parameters on the sensitivity of the impedance response. The control of the physical and dimensional characteristics of the sample is based on the measurement of the impedance changes. These changes will be presented in the plane of the standardized impedance, also called normalized impedance. This plane of impedance permits the trace of the standardized reactance as a function of the standardized resistance.

For simplicity, only an axisymmetric problem is considered, and the developed program will be applied to some plated aluminum samples (as shown in Fig. 1).

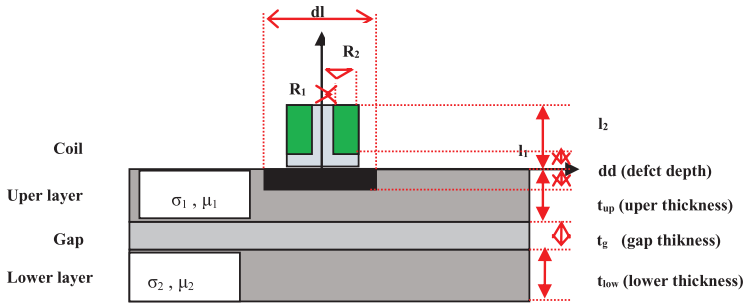

Figure 1: Description of the studied problem

2.2 Problem Modeling

However, it has been observed that the EC phenomenon is influenced by the skin effect, and the penetration depth increases as the frequency lowers [5,30–36]. The feeble value of frequencies seems to be most appropriate for hidden defect detection. Simulations could be carried out on a broad range of excitation frequencies, which range from a few Hz to a few kHz.

The standard penetration depth δ of the induced currents is given when the amplitude of the current density reaches (37%) of the surface density:

$$\delta = \sqrt{\frac{2}{\sigma \omega \mu}} \tag{1}$$

where ω is the excitation frequency, σ is the conductivity, and μ is the permeability of the target material.

Eq. (1) is often used to evaluate the penetration depth of the EC when an exciting probe is located on the top of a plate. The standard skin depth δ is approximately the thickness until the eddy currents penetrate. The effective penetration depth depends on the used instrument, probe type, permeability and conductivity of the tested domain and frequency of the probe excitation. It cannot be defined using the theory of the standard penetration depth based on the concept of a plane wave (i.e., Eq. (1) is a limited formula usable only for homogeneous conductive objects). Instead, it must be evaluated experimentally using test samples.

The EC modeling employs electromagnetic field interaction in all its applications. This interaction is governed by Maxwell's equations given as:

$$\mathrm{curlH} = \mathrm{J} + \partial \mathrm{D}/\partial \mathrm{t} \tag{2}$$

$$\mathrm{curlE} = -\partial \mathrm{B}/\partial \mathrm{t} \tag{3}$$

$$\mathrm{div.B} = 0 \tag{4}$$

$$\mathrm{div.E} = \rho/\varepsilon \tag{5}$$

where E is the electric field intensity, J is the current density ($\mathrm{J} = \sigma \mathrm{E}$), D is the electric displacement ($\mathrm{D} = \varepsilon \mathrm{E}$), B is the magnetic induction, H is the magnetic field intensity ($\mathrm{B} = \mu \mathrm{H}$), μ, σ, ε and ρ are the magnetic permeability, electric conductivity, electric permittivity and electric charge density of the selected domain, respectively.

However, to calculate the electromagnetic and EC fields, it is often simpler to introduce mathematical tools called potentials. These potentials permit the reduction of Maxwell's equations to partial differential equations. Several potential formulations appropriate to these problems can be distinguished. The electric formulation, also known as the A-V formulation, was chosen in this work. This formulation is based on the introduction of two unknown potentials as variables (the magnetic vector potential A and electric scalar potential V). The magnetic flux density B and the electric field E can be defined as:

$$B = \text{curl}A \tag{6a}$$

$$E = -\text{grad}V - \partial A/\partial t \tag{6b}$$

Substituting Eqs. (6a), (6b) and constitutive relations in Eqs. (2) and (3), derived Maxwell's equations can be expressed as:

$$\begin{cases} \text{curl}\,\dfrac{1}{\mu}\text{curl}A = -\sigma\left(\text{grad}V + \dfrac{\partial A}{\partial t}\right) - \dfrac{\partial}{\partial t}\varepsilon\left(\text{grad}V + \dfrac{\partial A}{\partial t}\right) \\ \text{curl}\left(\text{grad}V + \dfrac{\partial A}{\partial t}\right) = \dfrac{\partial}{\partial t}\text{curl}A \end{cases} \tag{7}$$

To obtain simple forms of these equations, the formula (rot (rot A) = –div (grad A) + grad (div A)) and Coulomb gauge condition (div A = 0) must be imposed. The EC problem can be described mathematically by Eqs. (8) and (9) which are given as the following:

$$\nabla^2 A + K^2 A = -\mu J \tag{8}$$

$$\text{div}.J = \text{div}\sigma(j\omega A + \text{grad}V) = 0 \tag{9}$$

where J is the excitation current density, μ is the magnetic permeability and σ is the electric permittivity. $\partial/\partial t$ is replaced by $j\omega$, $K^2 = -j\omega\mu(\sigma + j\omega\varepsilon_0)$ where ω denotes the angular frequency, j is the imaginary unit and ε_0 is the dielectric constant (More information and details can be found in [5,36–38]).

However, the objective of the EC problem resolution is to solve Eqs. (8) and (9). The potential A (in the entire domain of the considered problem) and electric potential V (in the conductive regions of this domain) will be calculated. The magnetic field H or magnetic induction B as well as the induced current, and impedance can be finally calculated.

2.3 FEM Formulation

The considered domain model consists of several regions that can be divided into four parts based on their magnetic and electric properties (see Fig. 1). The first part is the probe region. It can also be divided into two subparts (the circular coil part and the core part) and it is considered as an inducting region. The second part is the air region including the lift-off region if it exists, which is considered as a dielectric region. The third part is the gap region, which can be taken as an air gap region if air is used as a separator. Finally, the fourth part is the regions of conductive layers, which have their own magnetic and electric properties.

The differential equation in each region (inductive region/ conductive and non conductive region/ air region) represents a particular case of Eq. (8). The complete domain is governed by the entire system given as:

$$\nabla^2 A = \begin{cases} \mu\,(\sigma j\omega A - J_s) & \text{in conductor} \\ -\mu J_s & \text{in inductor} \\ 0 & \text{in air} \end{cases} \tag{10}$$

where J_s is the source current. The gradient of the potential V is implicit in J_s.

Eq. (9) can be rewritten in the conductive region as:

$$\nabla^2 V = -\,j\omega(\mathrm{div}A) \tag{11}$$

To ensure the uniqueness of the solution concerning Eqs. (8) and (9), it is necessary to include other types of conditions. Boundary conditions (the space conditions of Dirichlet and Neumann, and temporal conditions) as well as continuity conditions must be introduced.

A computational solution based on the FEM method must be carried out to determine the different unknowns of the problem. The formulation by the FEM method consists of double discretization, the mesh generation of the studied domain and the fields' discretization (formulation to partial derivative equations).

However, the study of thin structures in which one of the dimensions is weak entrains several difficulties in the mesh of the physical domain. The presence of deformed elements and obtaining condensed elements are the most apparent difficulties. In addition, the A–V potentials formulation generates an important number of unknowns in the system to be solved (four unknowns). To surmount these considerations, the mesh should not be too large to avoid vague results. Thus, the mesh should also not be too thin to avoid an increase in computing time. The use of degenerated elements can offer an appropriate solution to eliminate these problems. The specific elements employed to mesh the calculation zone are the tetrahedral Whitney elements. These elements are of the first order with several degrees of freedom at the nodes and edges. They were selected to overcome the difficulty that the modeling of low thickness structures poses.

The FEM computational model was implemented using the Galerkin formulation. This formulation allows the definition of interpolation functions N that describe the solution of the problem in the domain of resolution Ω. It explains that the projection of the solution on the space of the functions N is overall null on the domain of resolution Ω.

To obtain the magnetic vector A, these interpolation functions must be multiplied with the residual of Eq. (8) and integrated over the domain of resolution Ω. The weak formulation of Galerkin related to the EC problem is given as:

$$\int_{\Omega} N\left(\nabla^2 A + K^2 A + \mu J\right)\partial\Omega = 0 \tag{12}$$

where A is the solution of the problem (the vector magnetic in this case), Ω is the domain of resolution, N is the approximate function and ∇ is the mathematical operator.

Elemental solutions for each mesh element must be obtained. The domain of resolution Ω can be defined as an elemental surface or elemental volume depending on the formulation type (2D or 3D). Potentials A and V are approximated using the basis vector and scalar interpolation functions. The number of these basis functions corresponds to the number of nodes attached to the selected element for the meshing. The algebraic form of the elemental solution is expressed as:

$$A^e = \sum_{1}^{nn} N_i^e A_i^e \tag{13}$$

where N_i and A_i are the interpolation functions and the value of the potential function, respectively, and nn is the number of nodes of the mesh element. Each node can have a number of unknowns, so-called degrees of freedom. If the degrees of freedom FD in each node are greater than 1 (FD > 1), the number of nodes nn must be multiplied with FD (nn = nn. FD).

This elemental contribution enables the construction of a linear system of equations that gives the elemental matrix and vector components. This system is given as the following:

$$[[K_e] + j\sigma\omega\,[R_e]]\,\{A_e\} = \{b_e\} \tag{14}$$

where $[K_e]$ and $[R_e]$ are (nn.nn) matrices representing the real and imaginary parts of the stiffness matrix, respectively, $\{A_e\}$ is (nn.1) complex vector of unknowns and $\{b_e\}$ is (nn.1) complex vector of source currents.

The global system of equations must sum all elemental systems. It is given for the total number of nodes N by:

$$[KG]\,\{AG\} = \{QG\} \tag{15}$$

where $[KG] = [K] + j\,\sigma\omega[R]$ is the (N.N) banded symmetric complex global matrix, {QG} is the (N.1) complex source vector and {AG} is the (N.1) complex vector of unknowns.

Taking advantage of the symmetry and bandwidth of the global matrix [KG], an appropriate iterative algorithm was applied to resolve this system. The obtained solution enables the determination of the values of the magnetic potential A at the nodes of the studied domain mesh.

The values of the magnetic vector A and electric scalar V are simultaneously obtained after the numerical solution of the above algebraic system. From these values, other quantities can be deduced and calculated, such as the magnetic flux B, induced EC density Js, stored magnetic energy W, dissipated energy (or EC losses) P, etc.

The change in resistance R is associated with dissipated energy P and is given by the following expression:

$$R = \frac{P}{I^2} \tag{16}$$

The change in inductance L is associated with the stored energy W and is given by:

$$L = \frac{2W}{I^2} \tag{17}$$

The measurement of the numerical model for the coil impedance can be given in terms of the changes in resistance and inductance as the following:

$$Z = R + j\omega L \tag{18}$$

To ensure good control of the sensitivity of the impedance variations, it is possible to exploit the results using the standardized impedance. For that, the initial impedance Z0 (R0 + jX0) must be introduced. Z0 is obtained when the probe is not coupled with the material (sample or test target). The first measurement Z0 (X0, R0) must be taken relatively far from the sample, and the impedance is standardized as the ratio of the impedance Z and Z0 (Zs = (Z-R0)/X0).

The referential standardized impedance Zsf must be calculated first for a sample without defects to be used as a reference. The standardized impedance Zs of the coil placed on top of the sample with or without defects can be calculated next. The impedance difference ΔZ is formed by subtracting the

impedance Zs from Zsf ($\Delta Z = Zs - Zsf$). The variation in ΔZ reflects the influence of any change in problem parameters.

3 Application and Results

In this section, the computational simulation and analysis for the EC-NDT will be established and exploited through a code developed during this study. The electric formulation in the combined potentials was programmed and solved for the harmonic mode in the case of the treated problem.

The problem presented in Fig. 1 is taken as a test sample. It consists of two conductive layers, which are typically similar to those used in the construction of aeronautical structures. The electric conductivity is 17 MS/m and the relative permeability is 1 for each layer. A coil whose inner radius R_1, outer radius R_2, coil height t_h, and turns number n of 3, 6, 9 and 300 turns, respectively, is placed over the top layer with a given value of lift-off.

Simulations could be carried out on a broad range of excitation frequencies sweeping from 200 Hz to 200 kHz. The air gap thickness tg can take several values (0, 0.2, 0.4, 0.6, 0.8 and 1 mm).

3.1 Simulation Part 1: Modeling of a Thin Conductive Domain without Defect

3.1.1 Model Validation

The model validation is a very important step. The FEM modeling was implemented using a self-designed code developed by the authors. The Gauss elimination algorithm, which is an iterative process, was applied to solving the algebraic system.

Firstly, the code was applied to calculate the magnetic potential on a thin multilayer sample without the presence of defects. Once this potential is obtained, other parameters such as the current density, energy loss, and impedance are calculated.

The used samples are multilayer structures of the same material (aluminum alloy). The upper thickness t_{up} (top layer) and the lower thickness t_{low} (bottom layer) are taken as constant, $t_{up} = t_{low} =$ 1.5 mm. The electric conductivity is 17 MS/m and the relative permeability is 1 for each layer.

The lift-off is supposed to be null, and the tg value is $t_g = 0$ mm. This situation enables to consider the treated problem as a similar case to the conventional basis test of the EC probe above a massive simple.

Based on the Dodd and Deeds approach, the general analytical expression of the air coil impedance placed on multilayer conductors is given by:

$$z = \frac{j\omega\pi\mu nt^2}{(l_2 - l_1)^2(R_2 - R_1)^2} \int_0^{\infty} \frac{1}{\alpha^5} I(\alpha)^2 \left\{ 2\,(l_2 - l_1) + \frac{1}{\alpha}[2e^{-\alpha(l_2 - l_1)} - 2 + \left(e^{-\alpha l_1} - e^{-\alpha l_2}\right)^2 \varphi(\alpha)] \right\} \partial\alpha \tag{19}$$

with:

$$I\,(\alpha) = \int_{\alpha r_1}^{\alpha r_2} x J_i(x) \partial x \tag{20}$$

Eq. (20) is given in terms of integrals of Bessel functions.

$\phi(\alpha)$ is a complicated function involving the material properties of each layer (conductivity and permeability). Where α is the separation constant (spatial frequency), $\alpha_i = (\alpha 2 + j\omega\mu\sigma_i)^{1/2}$, nt is a constant number of turns, l_2 is the distance from the conductor to the top of the coil, l_1 is the distance from the conductor to the bottom of the coil, and R_1, R_2 and other geometrical data are exposed in Fig. 1.

To surmount the time consuming of the Dodd model, the model has also extended and developed in various recent papers. Using series expressions methods, integral expressions are represented as sums of higher transcendental functions. The series methods keep time and ensure better convergence without any sacrifice in terms of computational accuracy. More details about this analytical solution are described in several papers [3,14,27–33].

A comparison between calculated and analytical results is carried out in Fig. 2. The coil carries sinusoidal currents sweeping from 200 Hz to 200 kHz and some selected test values are presented on a logarithmic scale.

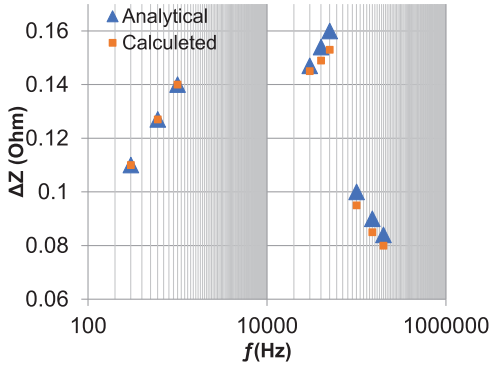

Figure 2: Impedance variations as a function of the excitation frequencies (analytical and calculated values)

Fig. 2 shows a remarkable agreement with the analytical results for all frequency ranges, from lower to higher frequencies. This agreement between the simulated signals and the analytical data is more significant in terms of impedance amplitude.

The numerical and analytical values are in the same trend, and they give the same trajectories.

- For low frequencies, less than <1 kHz, the average error is 0.17%.
- For frequencies ranging between 10 and 100 kHz, the average error is 3.2%.
- For higher frequencies, greater than >100 kHz, the average error is 5.3%. This increase in variation can be explained by the fact that it is difficult to describe the EC phenomena at high frequencies.

The normalized impedance and the impedance difference are recommended to obtain a better interpretation and exploitation of the small impedance variations. They are used in order to quantify the influence of various parameters.

It is important to record that the curve of standardized impedance versus the excitation frequency $\Delta Z(f)$ presents a nonlinear relationship for all frequency ranges. This liaison is indicated by the existence of various zones, which initially increase in a monotonic form and then decrease according to frequency increases. The choice of the relevant frequency range will depend on the constitutive parameters of the multilayer structure (thickness, materials, etc.). To obtain the best simulation implementation, it is necessary to choose frequencies located in the same zone. For the higher frequencies, the standard penetration depth becomes very low, and interactions with the deeper zones of structures are very low. A monotonic zone relating to low frequencies is desirable for cases of thin structures.

As mentioned in Fig. 3, the point where the evolution form of the curve $\Delta Z(f)$ undergoes changes can be used to identify an optimal frequency of operation. This frequency, denoted fopt, can be determined experimentally or through simulations.

Fig. 3 illustrates that for frequencies less than <5800 Hz the impedance increases as the frequencies increase. The trend curve is linear and presents a monotonic evolution of the curve $\Delta Z(f)$. Fig. 3 also shows that for frequencies greater than >5800 Hz (6000 Hz and more), the impedance decreases as the frequencies increase. The related trend curve of $\Delta Z(f)$ is linear and presents a monotonous decrease.

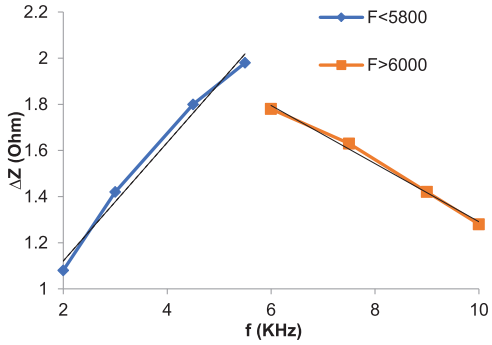

Figure 3: Evolution of ΔZ as a function of the excitation frequency

Simulations allow the consideration of the optimal frequency value of 5800 Hz. According to the parameters of the studied problem, it is interesting to measure Z at the frequencies located in monotonic zones related to this frequency.

Fig. 4 shows the evaluation of the magnetic induction B for a specific range of displacement (x [−0.6, 0.6] mm). This figure presents a comparison between calculated results and those given by the FEMM code. The parameters of the selected configuration are those of the sample used in the first part of this section.

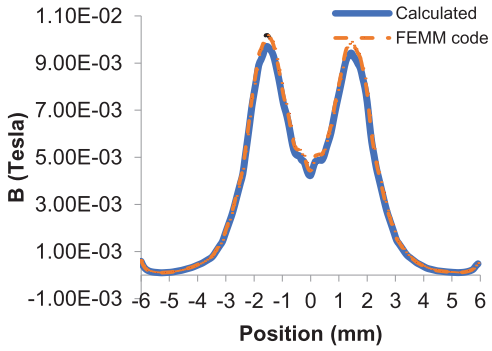

Figure 4: Evaluation of the magnetic induction B, comparison between calculated and FEMM results

The related mesh for this sample was realized with 4025 nodes and 7774 triangular elements for the FEMM code, and 2877 nodes and 1457 tetrahedral Whitney elements for the developed code.

Comparison to the FEMM results shows a good agreement and the average error obtained between both solutions is 5%. The accuracy of the developed code is in general satisfactory that making the expansion of the code to other simulations a realizable operation.

3.1.2 Effect of the Thickness of the Upper Layer

In this section, the upper thickness t_{up} takes different values (0.5, 1.0, 1.5 and 2.0 mm) and the chosen frequency is 2 kHz. The other test parameters are fixed (the same parameters quoted in the above section).

Fig. 5 presents a comparison between numerical results and those obtained from the analytical model. Thus, Fig. 6 shows the impedance variation ΔZ as a function of the upper thickness change.

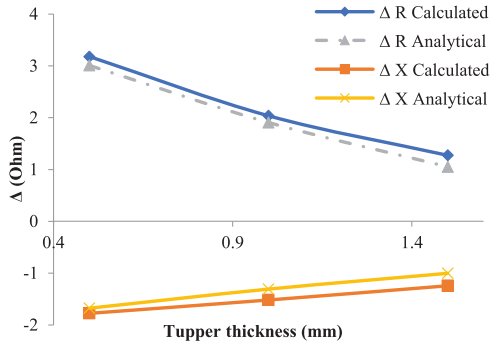

Figure 5: Variations of the resistance and reactance *vs.* the tup changes

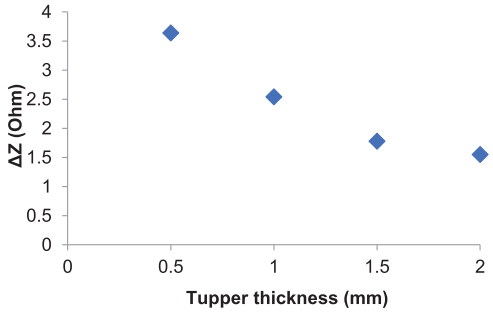

Figure 6: Impedance variations *vs.* the t_{up} changes for a fixed frequency of 2 kHz

Fig. 5 shows a good approximation for low values of the upper thickness ($t_{up} < 1$ mm). Compared to the analytical calculation, the reactance variation (the imaginary part of the impedance) similarly increases when t_{up} increases. On the other hand, the resistance variation (the real part of the impedance) decreases as t_{up} increases.

The average error is 15% for reactance calculations, and it is 5.17% in the case of resistance calculations. The value of the reactance changes by 28% and 30% if the upper thickness changes from 0.5 to 1 mm and from 1 to 1.5 mm, respectively.

Fig. 6 illustrates the impedance variation according to the effect of the upper thickness t_{up} change at a fixed frequency. The impedance decreases when the t_{up} increases.

The agreement of results shows that the calculated results are promising. The detection sensitivity is significant for the small value of the upper thickness. They can easily be used to determine the thickness of a conductive upper layer, especially to detect coating thicknesses above the substrate.

3.1.3 Effect of the Air-Gap

In this case, the considered sample consists of two conductive layers separated by an air gap. The thickness of the air gap may vary within a certain range. The conductivities of the two layers are the same (17 MS/m) and the relative permeability is 1 for each layer.

Considering for the first time, that the air-gap separating the layers has a null thickness $t_g = 0$ µm. Fig. 7 shows the evolution of the normalized impedance obtained for $t_{up} = 1.5$ mm, $t_{low} = 1.5$ mm, and $t_g = 0$ mm over a large frequency range [100–15,000 Hz].

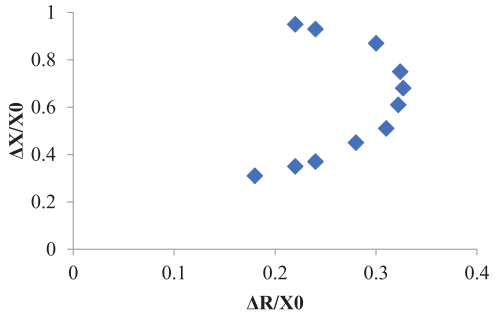

Figure 7: Normalized impedance plane for $t_g = 0$ mm, $t_{up} = 1.5$ mm and $t_{low} = 1.5$ mm

This figure illustrates the shape of the trajectory that describes the point of the probe impedance according to frequency variations. The determination of this trajectory for an unspecified material is a complex problem. This problem requires complete modeling and an important time of calculation. Any change in any parameter of the model induces a displacement of the representative point of impedance in this standardized impedance plane.

Fig. 7 shows the general curve of the normalized impedance for each possible simulation of the problem. This curve cannot quantify the impact of the selected parameter on the calculus sensitivity for only one simulation. Several curves must be combined in the same plane to obtain an appropriate analysis.

To evaluate the influence of the gap thickness on the impedance response, the thicknesses of the two layers must be fixed (1.5 mm for each layer). The gap thickness will be varied, and the first simulation presented in Fig. 7 can be taken as a reference. Fig. 8 represents the curves of normalized impedance obtained for thicknesses of the gap ranging between 0.0 and 1.0 mm with other parameters being fixed.

Fig. 8 gives a global idea of impedance evolution. The air gap thickness is the unique parameter that differentiates these simulations. Its effect on the impedance variation cannot be directly obtained from this figure. Thus, it is difficult to predict the relationship between the impedance variation and gap thickness due to the appearance of only small differences.

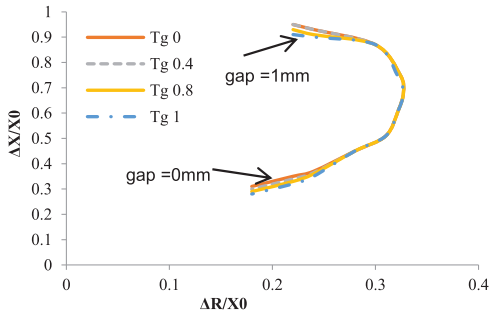

Figure 8: Normalized impedance plane ($t_{up} = 1.5$ mm, $t_{low} = 1.5$ mm, $t_g = [0.0, 0.4, 0.8$ and 1.0 mm], frequency range [100–15,000 Hz])

The zoom of this figure also proves that for low frequencies, the curves are arranged in an increasing order according to the gap thickness. The curve of standardized impedance established for the highest value of the gap thickness ($t_g = 1$ mm) is in front. For higher frequencies, it is the curve that corresponds to the lowest value ($t_g = 0$ mm) which is ahead. Therefore, there is a frequency range in which the properties of the normalized impedance are apt to allow gap thicknesses to be evaluated.

The determination of the relationship between the impedance variation and the gap thickness depends on several parameters. The type of this relationship is not always linear, due to the existence of several zones. In this study, a frequency range less than the optimal frequency (considered in the preceding section) was selected. The frequency of 5 kHz is used to analyze the effects of the gap thickness on the impedance variation.

Fig. 9 presents the evolution of ΔZ as a function of the gap thickness for a fixed frequency value [f= 5 kHz].

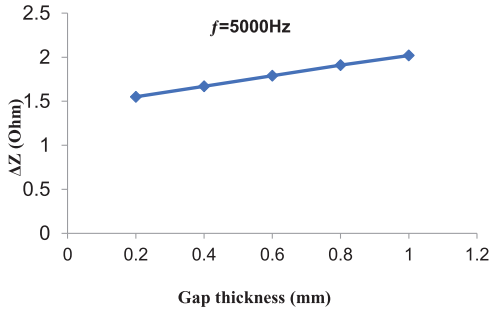

Figure 9: Evolution of ΔZ as a function of the gap thickness for a fixed frequency value

Fig. 9 illustrates that there is a certain frequency range where the function $\Delta Z(t_g)$ is expressed by a linear relationship. The slope of the representative line is equal to 0.6 according to the selected frequency [f = 5 KHz].

Therefore, there are several intervals of frequency where the variation of the standardized impedance is a linear function of the gap thickness. This linear relation can be deduced by calculating the slope of the obtained line. The deduced line is strongly related to the chosen frequency. However, it is very important to optimize the appropriate frequency in order to increase the sensitivity of EC signals in the presence of a gap.

3.2 Simulation Part 2: Modeling of a Thin Conductive Domain with a Defect

3.2.1 Effect of the Defect Length

The coil response will be formed by subtracting the impedance difference measured over an area containing two layers of aluminum alloy. The defect is located on the top surface of the upper layer. The thicknesses of the two layers are fixed (1.5 mm for each layer), the gap thickness is $t_g = 0.2$ mm, the lift-off is 0.1 mm and the frequency value is 2 KHz. The defect depth dd is 0.2 mm and the defect length dl changes are (4, 8, 10, 12 and 14 mm).

The influence of defect length changes on the impedance variation is illustrated in Fig. 10.

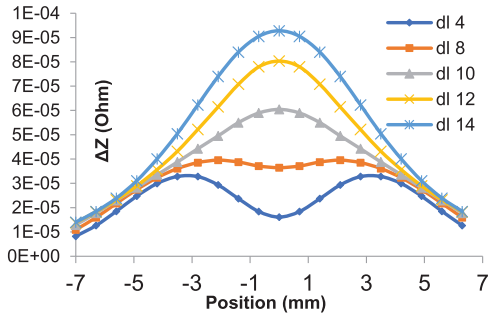

Figure 10: Effect of defect length on impedance variation

Fig. 10 shows that the effect of defect length changes is definitely apparent. The impedance increases as the defect length increases. Moreover, Fig. 10 indicates that the curves of the impedance variation do not have the same shape when the defect length increases. The shape of the impedance curve depends on the relationship between the defect length dl and the outer radius R_2. The impedance curve has a peak to valley form if $dl < 2.R_2$ and a peak form if $dl > 2.R_2$.

3.2.2 Effect of the Defect Position

In this case, two conductive layers with the same geometrical and electromagnetic characteristics represent the considered sample. The defect length and depth are taken as constants (dl = 12 mm and dd = 0.2 mm) and other parameters of the problem are fixed. The influence of the defect depth position can be represented by a series of defects located in various positions (see Fig. 11).

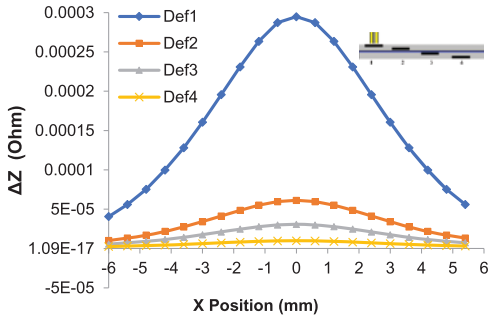

Figure 11: Effect of the defect location on impedance variation

The depth to be considered is the distance from the defect to the top surface of the upper layer connected to the coil. Fig. 11 shows that the increase in the depth of the defect position generates a

decrease in the impedance value. The impedance response is clearer for defect 1 located on the top surface of the upper layer. There is a reduction in the detection sensitivity for the defects (2, 3, and 4) compared to the case of defect 1.

This application confirms that the impedance variation strongly depends on the defect length and position. Thus, the information given by this variation, especially the impedance amplitude, can be used to identify and characterize the defect and its parameters.

3.2.3 Effect of the Excitation Frequency f

The evaluation of multilayer structures by the NDT-EC returns to determine the influence of the variation of various parameters on the probe response. This response is deferred to impedance changes, which can be done only with an adequate frequency.

In practice, the applied excitation frequencies cover a large range, going from a few Hz to a few MHz. Moreover, the selection of an adapted range with a definite problem is not always assured.

To illustrate the effect of the various parameters on the standardized impedance plane, the impedance variations must be highlighted in a certain frequency interval. The experimental studies and simulations in this field showed that the relation between the impedance and the excitation frequency is nonlinear. The curve Z(f) (Z as a function of frequencies) is not always monotonous.

However, there are initially two ranges: the first is that where the curve Z(f) increases (the impedance increases with the frequency). On the other hand, the second one decreases with the increase in frequency. An optimal frequency fopt must be introduced to distinguish these ranges (see the above sections).

As mentioned in Fig. 2, the trend of $\Delta Z(f)$ is not always linear. It is important to select frequencies included in zones of monotone evolution. In the frequency range $f < fopt$, the curve $\Delta Z(f)$ increases with the increase of frequency and it decreases if $f > fopt$.

In Fig. 12, the excitation frequencies included in the decreasing monotonous zone ($f > fopt$) are taken to realize simulations concerning this section. The considered sample is of two layers of aluminum where the upper layer thickness is 1.5 mm. The frequency range is [13, 50 kHz]. Other parameters are identical to those used in the previous example.

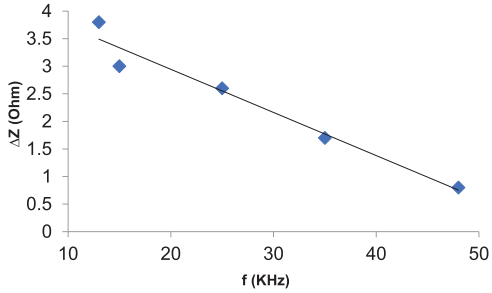

Figure 12: Variations of Z as a function of the excitation frequency, f [13,000–50,000 Hz]

In the selected range of the optimal frequencies, Fig. 12 shows that the normalized impedance decreases with the increase of the excitation frequency. In this zone, the variation trend of $\Delta Z(f)$ is linear, and the impedance value is inversely proportional to the frequency value.

The evolution of this simulation is similar to that of the first section (structure without defects). The presence of the defect generates a variation in the response of the impedance. So the first measurement can be used as a reference, allowing the detection of a defect's existence in a structure.

3.2.4 Effect of the Thickness of the Lower Layer

Fig. 13 illustrates the impedance variation as a function of the lower thickness change. The upper thickness t_{up} is taken as constant ($t_{up} = 1.5$ mm), the lower thickness t_{low} takes different values (0.5, 1.0, 1.5 and 2.0 mm), and the chosen frequency is 2 kHz. The other test parameters are fixed (the same parameters quoted in the above sections).

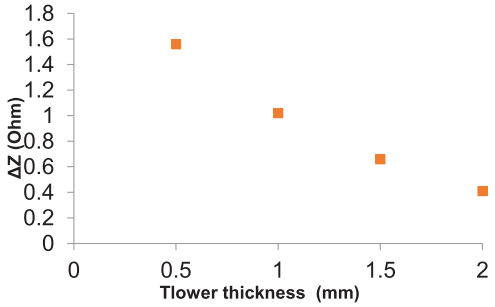

Figure 13: Impedance variations *vs.* t_{low} changes

Fig. 13 shows that for a fixed frequency, the measurement of ΔZ is more sensitive when the lower thickness t_{low}, is higher. Realized simulations enable the estimation of influences of various thicknesses on a multilayer structure. A fixed upper layer and a bottom layer of unknown thickness feature this configuration. Simulation can be applied to multilayer structures with or without defects in a chosen (optimal) range of frequency.

While carrying out this standardization, the measurement becomes independent of the particular characteristics of the excitation coil (number of turns and energy losses). It only depends on the frequency of excitation, coil geometry, distance (lift-off) and the geometrical and electromagnetic parameters of the tested target.

4 Conclusion

Eddy current testing is very challenging. The impedance signals are functions of the geometrical dimensions and mechanical and electromagnetic properties of the tested material. They are also influenced by the probe design.

The numerical model studied in this paper enables the prediction and evaluation of important parameters. These parameters directly affect the impedance responses of eddy current testing used for low thickness multilayer structures.

Realized simulations can estimate the influences of certain parameters (air-gap thickness, upper layer thickness, lower layer thickness, excitation frequency, etc.) on the EC inspection of a multilayer structure. Indeed, the chosen parameters can be changed and entered automatically, and responses versus different frequencies can be obtained.

Simulations show that the curves of the standardized impedance variation according to certain parameters are linear. However, for the majority of these parameters, the evolution of ΔZ is linear and

proportional. The variation of the slope of these lines depends on the effect of changes in the value of these parameters.

These variations of the standardized impedance are highlighted at certain frequency intervals based on the changes in various parameters. They could be exploited for the evaluation of multilayer structures presenting changes in a chosen parameter among the group of selected parameters.

This approach can be adapted and developed to be used for the estimation of thicknesses between parts in aeronautical multilayer structures. It can also be used for any similar problem consisting of a fixed upper thickness and a fixed excitation frequency.

The simulations and curves obtained can serve as solid support for constructing databases. These reference databases will be very useful for the determination of empirical relations between various parameters and excitation frequency. These relations are obtained through interpolation or extrapolation functions relating to the various curves and can be applied to solve inverse problems.

The proposed method in this paper is a promising measurement tool to optimize the coil design. It can be used to approximate the ideal excitation field to obtain the best level of control. However, further work must be performed to enrich knowledge and ameliorate the performance of the NDT-EC method.

Acknowledgement: None.

Funding Statement: The authors received no specific funding for this study.

Author Contributions: The authors confirm contribution to the paper as follows: study conception and design: Salim Bennoud; data collection: Salim Bennoud, Elkhahina Sari; analysis and interpretation of results: Salim Bennoud; draft manuscript preparation: Salim Bennoud, Elkhahina Sari. All authors reviewed the results and approved the final version of the manuscript.

Availability of Data and Materials: Not applicable.

Ethics Approval: Not applicable.

Conflicts of Interest: The authors declare no conflicts of interest to report regarding the present study.

References

1. Weiying C, Hidetoshi H. Characterization of multilayered structures by swept-frequency eddy current testing. AIP Adv. 2019;9:035009. doi:10.1063/1.5079959.
2. Du W, Bai Q, Wang Y, Wang Y, Zhang B. Eddy current detection of subsurface defects for additive/subtractive hybrid manufacturing. Int J Adv Manuf Technol. 2018;95(9):3185–95. doi:10.1007/s00170-017-1354-2.
3. Tytko G. An eddy current model of pot-cored coil for testing multilayer conductors with a hole. Bull Pol Acad Sci Tech Sci. 2020;68(6):1311–7. doi:10.24425/bpasts.2020.135388.
4. Ye B, Dong J, Qiu G, Li S, Zeng F, Yang T, et al. Eddy current inversion models for estimating dimensions of defects in multilayered structures. Math Probl Eng. 2014;2014(1):649608. doi:10.1155/2014/649608.
5. Bennoud S, Zergoug M. Modeling and simulation of defects inspection in conductive multi-layered pieces by the eddy current technique. J Phys: Conf Series. 2015;574:012095. doi:10.1088/1742-6596/574/1/012095.
6. Abdou A, Safer OA, Bouchala T, Bendaikha A, Abdelhadi B, Guettafi A, et al. An eddy current nondestructive method for crack detection in multilayer riveted structures. Instrum Mesure Metrologie. 2019;18(5):485–90. doi:10.18280/i2m.180508.

7. Sari E, Benachenhou K, Bennoud S, Halimi R, Mimouni O. FSW'S ultrasonic method for determining residual stresses in welded aeronautical structures. Int J Mech Product Eng. 2023;11(11):1–8.
8. Hidayat M, Chiang C, Yen M. Determination of the defect's size of multi-layer woven CFRP based on its temperature profile. Int J Appl Sci Eng. 2023;20(3):1–3. doi:10.6703/IJASE.202309_20(3).003.
9. Olga W, Wiera O, Michał M. Reconstruction of size and depth of simulated defects in austenitic steel plate using pulsed infrared thermography. Infrared Phys Technol. 2012;55(4):363–7.
10. Fan X, Yu J, Chen T. Research on crack monitoring technology of multilayer structure based on TMR-eddy current sensor. J Phys: Conf Ser. 2021;1986:012053.
11. Ye B, Li M, Qiu G, Dong J, Zeng F. Quantitative estimating size of deep defects in multi-layered structures from eddy current NDT signals using improved ant colony algorithm. Frattura ed Integrità Strutturale. 2014;28(8):32–41. doi:10.3221/IGF-ESIS.28.04.
12. Long TC, Thinh DD, Phuong CN, Thanh DB. A model-based approach for estimation of the crack depth on a massive metal structure. Meas Control. 2018;51(5–6):182–91. doi:10.1177/0020294018778314.
13. Tuna Gürbüz I, Rasilo P, Martin F, Osemwinyen O, Belahcen A. 2-D analytical model for computing eddy-current loss in nonlinear thick steel laminations. IEEE Trans Magn. 2022;58(9):1–4.
14. Xia Z, Huang R, Chen Z, Yu K, Zhang Z, Salas-Avila JR, et al. Eddy current measurement for planar structures. Sensors. 2022;22(22):8695. doi:10.3390/s22228695.
15. Uchanin V. Detection of the fatigue cracks initiated near the rivet holes by eddy current inspection techniques. Trans Aerospace Res. 2020;2020(2):47–58. doi:10.2478/tar-2020-0010.
16. Khebal M, Abdou A, Bouchala T, Aboura A, Bachir A, Amor G. Non-destructive rapid defect testing around curved head rivets without displacement of eddy current sensors. Stud Eng Exact Sci. 2024;5(1):2040–62. doi:10.54021/seesv5n1-101.
17. Sari E, Benachenhou K. Stress influence to eddy current control of cracked aeronautical material. J Meas Eng. 2021;9(4):231–40. doi:10.21595/jme.
18. Bennoud S, Zergoug M. Modeling and simulation of defects due to corrosion in turbine blades of turbojet. In: *6th International Symposium on NDT in Aerospace*, 2014 Nov 12–14; Madrid, Spain; 2014.
19. Uchanin V. Enhanced eddy current techniques for detection of surface-breaking cracks in aircraft structures. Trans Aerospace Res. 2021;1(262):1–14. doi:10.2478/tar-2021-0001.
20. Janovec M, Smetana M, Bugaj M. Eddy current array inspection of Zlin 142 fuselage riveted joints. Transp Res Procedia. 2019;40:279–86. doi:10.1016/j.trpro.2019.07.042.
21. Benmoussa OS, Ayad Ahmed N, Bouchala T. A comparative study of optimization methods for eddy-current characterization of aeronautical metal sheets. Facta Univ Ser Electron Energ. 2021;34(4):547–55.
22. Chady T, Okarma K, Mikołajczyk R, Dziendzikowski M, Synaszko P, Dragan K. Extended damage detection and identification in aircraft structure based on multifrequency eddy current method and mutual image similarity assessment. Materials. 2021;14(16):4452. doi:10.3390/ma14164452.
23. Vaverka F, Smetana M, Gombarska D, Janousek L. Diagnosis of artificial flaws from eddy current testing signals based on sweep frequency non-destructive evaluation. Appl Sci. 2022;12(8):3732. doi:10.3390/app12083732.
24. Khebal M, Abdou A, Bouchala T, Aboura A, Belkhiri K, Amor G. Static eddy current imaging for nondestructive testing of aeronautical structures. Stud Eng Exact Sci. 2024;5(1):3484–501. doi:10.54021/seesv5n1-173.
25. Janovec M, Čerňan J, Škultéty F. Use of non-destructive eddy current technique to detect simulated corrosion of aircraft structures. KOM-Corrosion Mater Protect J. 2020;64(22):52–8. doi:10.2478/kom-2020-0008.
26. Dodd CV, Deeds WE. Analytical solutions to eddy-current probe-coil problems. J Appl Phys. 1968;39(6):2829–38. doi:10.1063/1.1656680.

27. Sardellitti A, Di Capua G, Laracca M, Tamburrino A, Ventre S, Ferrigno L. A fast ECT measurement method for the thickness of metallic plates. IEEE Trans Instrum Meas. 2022;71:6004712. doi:10.1109/TIM.2022.3188029.
28. Juillard J, de Barmon B, Berthiau G. Simple analytical three-dimensional eddy current model. IEEE Trans Magn. 2000;36(1):258–66. doi:10.1109/20.822536.
29. Zhang J, Yuan M, Xu Z, Kim HJ, Song SJ. Analytical approaches to eddy current nondestructive evaluation for stratified conductive structures. J Mech Sci Technol. 2015;29(10):1–7. doi:10.1007/s12206-015-0910-7.
30. Koliskina V, Volodko I. Analytical solution of eddy current problems for multilayer medium with varying electrical conductivity and magnetic permeability. Int J Math Models Methods Appl Sci. 2013;7(2):174–81.
31. Theodoulidis T, Kriezis EE. Application of the TREE method to axisymmetric problems. In: Eddy current canonical problems (with Applications to Nondestructive Evaluation). Henderson, NV, USA: Tech Science Press; 2006.
32. Rucker WM, Hoschek R, Richter KR. Various BEM formulations for calculating eddy currents in terms of field variables. IEEE Trans Magn. 1995;31(3):1336–41. doi:10.1109/20.376274.
33. Assous F, Ciarlet P, Labrunie S. Mathematical foundations of computational electromagnetism. Cham, Switzerland: Springer; 2018. doi:10.1007/978-3-319-70842-3.
34. Huang R, Lu M, Chen Z, Shao Y, Xia Z, Hu G, et al. A novel acceleration method for crack computation using finite element analysis in eddy current testing. IEEE Trans Instr Meas. 2022;71:1–9. doi:10.1109/TIM.2022.3186073.
35. Athanasios K, Theodoulidis T. Hybrid model for eddy current testing defect detection in high frequencies. In: Electromagnetic non-destructive evaluation (XXIV). Amsterdam, Netherlands: IOS Press; 2023. p. 30–7. doi:10.3233/SAEM230006.
36. Bennoud S, Zergoug M, Allali A. Numerical simulation for cracks detection using the finite elements method. Int J Multiphys IJM. 2014;8(1):1–10. doi:10.1260/1750-9548.8.1.1.
37. Bennoud S, Sari E. Modeling of eddy currents problem using the shells elements method. In: *Mathematics and Information Technologies: Research and Education 2023 Conference*, 2023; Chişinău, Moldova.
38. Chen J, Chen Z, Cui T, Zhang L. An adaptive finite element method for the eddy current model with circuit/field couplings. SIAM J Sci Comput. 2010;32(2):1020–42. doi:10.1137/080713112.
39. Su Z, Ye C, Tamburrino A, Udpa L, Udpa S. Optimization of coil design for eddy current testing of multilayer structures. Int J Appl Electromagn Mech. 2016;52(1):315–22. doi:10.3233/JAE-162030.